Bulletin of the Seismological Society of America. Vol. 68, No. 5, pp. 1399–1413, October 1978

CRUSTAL STRUCTURES INFERRED FROM RAYLEIGH-WAVE SIGNATURES OF NTS EXPLOSIONS

BY THOMAS C. BACHE, WILLIAM L. RODI, AND DAVID G. HARKRIDER

ABSTRACT

An improved method for determining plane-layered earth models that accurately represent the important features controlling the amplitude and wave form of surface waves is presented. The method includes a formal inversion of phase and group velocity data determined from observed seismograms and is applied to the Rayleigh waves from Nevada Test Site (NTS) explosions recorded at Albuquerque, New Mexico and Tucson, Arizona. For both paths the observed dispersion agrees with that from the models with a maximum residual of only 0.01 km/sec. Further, the models are consistent with other available information about these paths (e.g., from refraction surveys). To properly account for local differences in the material at the source, an approximate theory is constructed in which the amplitude excitation is computed in a source structure and the dispersion in a separate path structure. Using this theory and the crustal models from the inversion, synthetic seismograms are computed that match the observed seismograms remarkably well.

INTRODUCTION

We present an improved method for determining plane-layered earth models that accurately represent the important features controlling the amplitude and wave form of the Rayleigh waves propagated along particular paths. Since dispersion data provide valuable information about earth structure, it is desirable to develop effective inversion techniques for interpreting them. Further, the better our models account for path effects, the more confidently we can relate the amplitudes of Rayleigh waves to source parameters, source structure, and dissipation effects. This is particularly important in problems related to the monitoring of underground nuclear explosions.

As an application, we use Rayleigh wave recordings of Nevada Test Site (NTS) explosions at the WWSSN stations ALQ (Albuquerque, New Mexico) and TUC (Tucson, Arizona) to infer the crustal structure for the NTS-ALQ and NTS-TUC paths. These paths, or portions of them, have been previously studied using body waves (e.g., Prodehl, 1970; Warren, 1969; Langston and Helmberger, 1974) and surface waves (e.g., Keller *et al.*, 1976; Alexander, 1963; Wickens and Pec, 1968) and these previous solutions provide a useful check.

Our inversion method includes a direct determination of phase and group velocities from the recorded Rayleigh waves and a formal linear inversion of these data for earth structure. It is similar to previously applied techniques (e.g., Keller *et al.*, 1976), but represents an extension and improvement.

Since both phase- and group-velocity data are used, our data have considerably greater resolving power than do group velocities alone. Also, the formulation and solution of the inversion problem is done by a more efficient and flexible method than previously used. Further, an interesting corroboration of the models is that theoretical seismograms computed with them show remarkable agreement with the observations.

Both phase and group velocities can be rather easily determined from explosion recordings because the phase and group delays at the source are nearly zero. The

methods used for determining group velocities (narrow band filtering) and phase velocities (unwrapping the phase spectrum) produce nearly independent estimates for the two. Nonetheless, we find the values for these paths to be quite consistent from event to event and in excellent agreement with the differential relationship between phase and group velocity.

The earth models found by the inversion are rather simple and are consistent with refraction data where it is available. The NTS-TUC path is characterized by a crustal thickness of 31 km and the average crustal thickness for NTS-ALQ is 42 km. The phase- and group-velocity data are all fit within 0.01 km/sec. The phase-velocity data are especially important if theoretical seismograms are to match the observations, as they do here. For example, a seismogram, its negative and its Hilbert transform all have the same group-velocity dispersion.

To compute synthetic seismograms, we must address the fact that conventional surface-wave theories (e.g., Harkrider, 1964) cannot be used in a consistent way when events in close proximity occur in different source materials, as is common at NTS. Therefore, we begin by constructing, albeit in a somewhat *ad hoc* way, a theory in which two structures are used to model the source-receiver travel path. The amplitude excitation is computed in a source structure and the dispersion is computed in a separate path structure. A transmission coefficient accounts for passage of Rayleigh waves between the two.

Rayleigh Waves from Proximate Events in Dissimilar Source Materials

A computationally convenient formulation of the theory for the surface waves generated by a point source in a plane-layered earth model was given by Harkrider (1964, 1970). The formulation of the theory is entirely in terms of linear elasticity, although the effect of anelastic attenuation can be included via an empirically determined Q operator. The source representation may be in terms of elementary point forces (Harkrider, 1964) or a general expansion of the outgoing elastic waves in terms of spherical harmonics (Harkrider and Archambeau, 1978). For spherically symmetric explosions a convenient source representation is the reduced displacement potential $\Psi(\tau)$ defined by

$$u(R, t) = -\frac{\partial}{\partial R}\left(\frac{\Psi(\tau)}{R}\right),$$
$$\tau = t - R/\alpha, \tag{1}$$

where u is radial displacement, t is time, α is the P-wave velocity, and R is the distance from the explosion.

For direct application of the theory the entire source-receiver travel path is modeled as a single plane layered medium. The Fourier-transformed vertical component of the fundamental mode Rayleigh wave generated by an explosion at depth h is then

$$\hat{w}(r, \omega) = -4\pi\mu_s \hat{\Psi}(\omega)\frac{K_s(h)\mathbf{A}_R}{c} H_0^{(2)}\left(\frac{\omega r}{c}\right), \tag{2}$$

where

$$K_s(h) = \frac{1}{2\mu_s}\frac{\sigma_s^*(h)}{\dot{\omega}_0/c} - \frac{\dot{u}_s^*(h)}{\dot{\omega}_0},$$

and the stress and displacement eigenfunctions are defined by Harkrider (1964, 1970). In equation (2) μ_s is the shear modulus of the source layer, r is epicentral distance, c is the phase velocity, $\dot{\Psi}$ is the time derivative of Ψ and a positive w displacement is upward. The amplitude response of the layered medium is represented by the real, positive quantities $\mathbf{A}_R$, which is source-depth independent, and $K_s(h)$. Harkrider (1970) tabulates c, $\mathbf{A}_R$, and the terms in K_s for several representative earth models. Finally, to account for anelastic attenuation and the sphericity of the earth, $\hat{w}(r, \omega)$ is multiplied by

$$e^{-\gamma r}\left(\frac{r}{a_e \sin \Delta}\right)^{\frac{1}{2}}, \tag{3}$$

where γ is an empirically determined attenuation factor, Δ is range in degrees, and a_e is the radius of the earth.

Using equation (2), amplitudes cannot be computed in a consistent way when the material near the source is not the same as that at the source depth in the average path model. This problem is particularly important in nuclear explosion seismology where there is considerable interest in the relative amplitudes of surface waves from explosions detonated in a wide variety of source materials (e.g., tuffs and granites at the Nevada Test Site).

A natural way to compare events in close proximity, but in different source materials, is to use two earth models, one for the source region and one for the remainder of the path. Alewine (1974) gives an approximate transmission coefficient that accounts for propagation of Rayleigh waves across a vertical boundary. It is based on results given by McGarr (1969) and McGarr and Alsop (1967). Using this, the equation for explosion generated Rayleigh waves in a two-structure earth model is

$$\begin{aligned}\hat{w}(r, \omega) = &- 4\pi\mu_s \hat{\dot{\Psi}}(\omega) \frac{K_{s_1}\mathbf{A}_{R_1}}{c_1} T(\omega)\, H_0^{(2)}\left(\frac{\omega r_1}{c_1} + \frac{\omega r_2}{c_2}\right) \\ &\times \exp\left(-\gamma_1 r_1 - \gamma_2 r_2\right)\left(\frac{r_1 + r_2}{a_e \sin\left(\Delta_1 + \Delta_2\right)}\right)^{\frac{1}{2}}\end{aligned} \tag{4}$$

where the source and receiver portions of the path are denoted by subscripts 1 and 2, respectively.

The transmission coefficient, $T(\omega)$, is derived by assuming the total horizontal energy flux remains constant during the transmission of Rayleigh waves across the boundary and is

$$T(\omega) = \left(\frac{c_2\, \mathbf{A}_{R_2}}{c_1\, \mathbf{A}_{R_1}}\right)^{\frac{1}{2}}. \tag{5}$$

The derivation assumes no mode conversion and includes no refraction effects.

For comparing events in close proximity as at NTS, we note the following points. First, known structural differences are restricted to the top few kilometers of the crust. Thus, at least for long periods, the boundary is nearly transparent and $T(\omega)$ plays a minor role since it is near unity. Second, it is reasonable to let $r_1 \rightarrow 0$ because the dispersion and attenuation are average path quantities that, to the extent they are derived from events in the source region under study, already incorporate any

mixed path effects that might be present. These points will be clarified by some examples in later sections.

Letting $r_1 \rightarrow 0$ in equation (4), the formula to be used for computing the surface waves from underground explosions becomes

$$\hat{w}(r, \omega) = -4\pi\mu_s \dot{\hat{\Psi}}(\omega) \frac{K_{S_1} \mathbf{A}_{R_1}}{c_1} T(\omega) H_0^{(2)}\left(\frac{\omega r}{c_2}\right) e^{-\gamma r} \left(\frac{r}{a_e \sin \Delta}\right)^{\frac{1}{2}}, \quad (6)$$

where r is the range and the other quantities are as in equation (4). With this formulation a single average path model can be used for all events in a region while accounting for changes in the local source material in a consistent way.

Surface-Wave Dispersion for NTS-Albuquerque and NTS-Tucson

Data from the WWSSN stations ALQ and TUC were collected for a number of NTS explosions. A striking characteristic of these data was the consistency of the

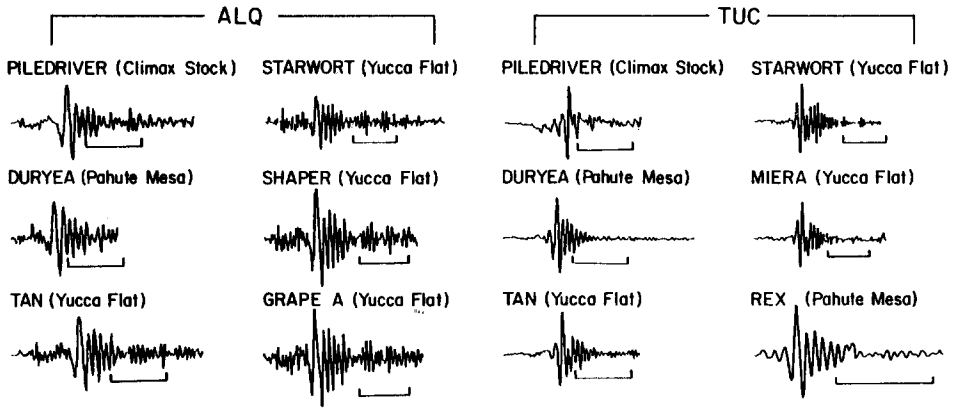

FIG. 1. Typical seismograms are shown for six events recorded at each station. The first three events in each column are plotted from hand-digitized data while the others are tracings from the film records. All seismograms are not on the same time scale—1 min is indicated on each record.

wave forms at each station. For example, the period of the maximum phase was measured for some 56 events recorded at ALQ and was found to be 11.0 ± 0.5 sec. The analogous period for 59 events observed at TUC was 8 ± 0.5 sec. Some typical examples are shown in Figure 1. The pertinent data for these events are summarized in Table 1 (from Springer and Kinnaman, 1971).

The path dispersion characteristics were determined by analysis of three representative recordings at each station, those for events PILEDRIVER, TAN, and DURYEA. These events were in three geophysically distinct testing areas at NTS and their surface waves represent the range of variation seen at ALQ and TUC. The six seismograms were digitized by hand from reproductions of the WWSSN film chips.

The phase and group velocities for the seismograms were determined using a computer program (Multiple Arrival Recognition System, MARS) developed primarily by C. B. Archambeau and described in several Systems, Science and Software contract reports (e.g., Bache *et al.*, 1976). In this program each seismogram is Fourier transformed and filtered by a narrow-band, Gaussian filter. The inverse-transformed narrow-band output and its Hilbert transform are constructed to obtain

TABLE 1

DESCRIPTION OF SELECTED EVENTS

Name and Date	Shot Time (GMT)	Yield (kt)	Depth (km)	Source Area and Material	TUC		ALQ	
					Azimuth	Distance	Azimuth	Distance
PILEDRIVER 6/2/66	1530:00:09	≈56	0.463	Climax Stock Granite	137°	728.1	103°	900.4
TAN 6/3/66	1400:00:04	Low-Intermediate	0.544	Yucca Flat Tuff	136°	714.1	102°	894.7
DURYEA 4/14/66	1413:43:10	65	0.560	Pahute Mesa Rhyolite	135°	752.6	103°	933.2
STARWORT 4/26/73	1715:00:16	85	0.564	Yucca Flat Tuff	136°	719.9	103°	898.0
SHAPER 3/23/70	2305:00:04	Low-Intermediate	0.561	Yucca Flat Tuff	136°	714.7	103°	893.9
MIERA 3/8/73	1610:00:19	Low-Intermediate	0.569	Yucca Flat Tuff	136°	716.4	103°	894.8
GRAPE A 12/17/69	1500:00:04	Low-Intermediate	0.551	Yucca Flat Tuff	136°	713.3	103°	892.1
REX 2/24/66	1555:07:04	16	0.672	Pahute Mesa Tuff	135°	755.0	103°	934.2

the envelope as a function of time. The peaks of the envelope function occur at the group arrival times of energy in a narrow band of frequencies near the filter center frequency. Generally, the narrower the filter, the less the contamination by energy from adjacent frequencies, but the less accurate the arrival time determination. For this reason each seismogram was analyzed using several filter widths. The group velocity was then determined as a function of period for each seismogram, assuming zero group delay at the source.

Using the far-field approximation for the Hankel function in equation (6), the Rayleigh wave phase delay is

$$T = T_s + \frac{r}{c_2} + \frac{3\pi}{4\omega}, \tag{7}$$

where T_s is the phase delay associated with the source function $\dot{\Psi}(\omega)$. Theoretical (e.g., Bache *et al.*, 1975) and empirical (e.g., Haskell, 1967) studies of the source find

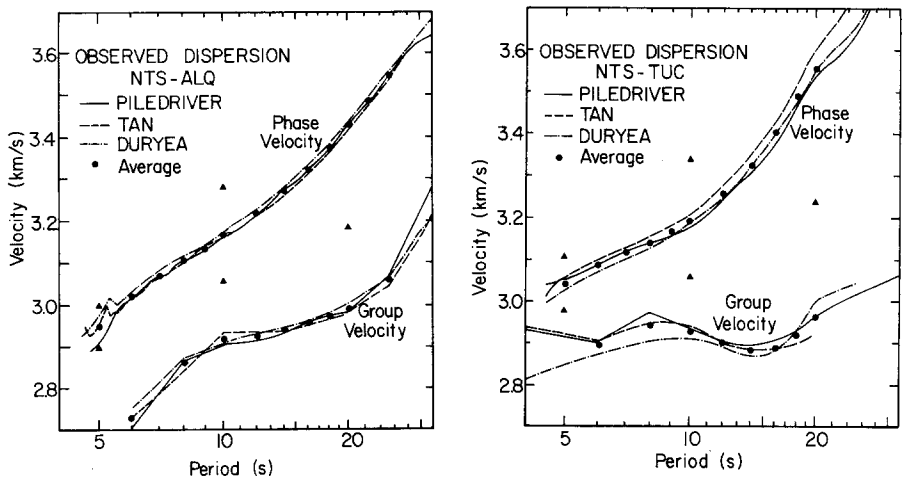

FIG. 2. The observed phase and group velocities are shown for three events at NTS to ALQ (*left*) and TUC (*right*). The lines denote the values determined from each event, while the closed circles are the average values used in the inversion. The closed triangles are the phase velocities implied by using values for n in equation (8) $\pm$ 1 different from those actually used.

T_s to be no more than a few tenths of a second at periods in the range of interest, so it can safely be ignored. Phase velocity is then determined by unwrapping the phase of the Fourier-transformed seismogram (removing jumps of 2π) and substituting into

$$c_2 = \frac{-r\omega}{\phi + \frac{3\pi}{4} + 2n\pi}, \tag{8}$$

where ϕ is the unwrapped phase and n is an integer selected to give reasonable values for c_2. The phase- and group-velocity data determined from each seismogram are plotted in Figure 2 together with the average values for each path. The phase velocities for n being ± 1 from the value chosen are also indicated. These phase velocities lead to unrealistic earth models.

Comparing the phase and group velocities, we see that they both are remarkably constant from event to event, especially for the NTS-ALQ path, and appear to provide equally accurate data sets. Since the two velocities were determined using entirely different methods, an excellent check is that they are found to agree closely with the relationship

$$\frac{1}{U_2} = \frac{d}{d\omega}\left(\frac{\omega}{c_2}\right), \tag{9}$$

where U_2 is the group velocity.

Earth Structure from Inversion of Surface-Wave Phase and Group Velocity

Systematic linear inversion is an effective method for inferring the average earth structure along a surface-wave path from its observed dispersion. The method determines an optimal earth model fitting the data and, in addition, offers a description of the uniqueness of the model and hence the resolving power of the data.

We assume the structure can be approximated by a plane-layered elastic model, described by velocities α, β, and density ρ as functions of depth z. The effects of lateral variations and anelasticity are not modeled. Linear inversion finds a model $(\hat{\alpha}, \hat{\beta}, \hat{\rho})$ whose values at each depth are estimates for spatial averages of the true structure. The accuracy of the $(\hat{\alpha}, \hat{\beta}, \hat{\rho})$ and the depth intervals over which the true structure is averaged are outputs of the inversion.

A limited number of fundamental-mode Rayleigh-wave phase and group velocities in a finite frequency band do not provide enough information to determine α, β, and ρ individually. The data dependence on α and ρ is weak compared to that on β. Therefore, we assume that α and ρ are linearly related to β and set

$$\begin{aligned} \hat{\alpha}(z) &= C_{1\alpha}(z)\,\hat{\beta}(z) + C_{2\alpha}(z), \\ \hat{\rho}(z) &= C_{1\rho}(z)\,\hat{\beta}(z) + C_{2\rho}(z), \end{aligned} \tag{10}$$

where $C_{1\alpha}$, $C_{2\alpha}$, $C_{1\rho}$, and $C_{2\rho}$ are prescribed. This allows a considerable flexibility for specifying α, ρ, Poisson's ratio, or other functions of the model at various depths. The inverse problem is then reduced to finding an optimal estimate for β.

An optimal model fulfills three objectives: it fits the data within their experimental uncertainty, is consistent with other available information about the regional structure, and it is as simple as possible while satisfying the first two objectives. Linear inversion accomplishes these objectives by simultaneously maximizing the fit to the data and the "smoothness" of the model. Many smoothness criteria have been used in geophysical inverse problems; for example, Backus and Gilbert (1970), Jordan (1973), Johnson and Gilbert (1972), Wiggins (1972). Our method for solving for $\hat{\beta}$ has features in common with these, but differs in some important aspects.

A commonly used smoothing criterion is to minimize $|\hat{\beta} - \beta_0|$, where β_0 is a guess model that is consistent with other available information. We use a different approach that is based on ideas introduced by Johnson and Gilbert (1972) and Jordan (1973). In our method other information, such as that from body-wave studies, is incorporated through the constraints in equation (10). We also specify the depths at which discontinuities in α, β, ρ are known or believed to exist. Our

smoothness criterion is then to minimize $|d\hat{\beta}/dz|$ in the segments between discontinuities. Neither the average value of $\hat{\beta}$ in a segment nor the jump in value across a discontinuity is restricted. This increases the number of degrees of freedom available for fitting the data while maintaining the simplicity of the model.

Since the functionals relating phase and group velocity to (α, β, ρ) are nonlinear, they are approximated by linear expansions about a reference model in terms of first-order partial derivatives and $\hat{\beta}$ is found by iteration. With our smoothness criterion, $\hat{\beta}$ depends on the reference model only indirectly through the partial derivatives.

For numerical implementation, the method is applied to models with a finite number of plane horizontal homogeneous layers. Theoretical dispersion is evaluated by the method described by Harkrider (1964). With this technique, exact phase velocity partial derivatives with respect to α, β, and ρ can be expressed in terms of energy integrals (Takeuchi *et al.*, 1964). Approximate but accurate group velocity partial derivatives are obtained by a numerical scheme due to Rodi *et al.* (1975).

A number of previous studies have suggested models for the crust along the NTS-TUC path. Refraction lines have been run along much of this path and have been studied by Diment *et al.* (1961) and Langston and Helmberger (1974). The latter study used both amplitude and travel-time information from the refraction seismograms and supplemented this with group velocity dispersion determined from TUC surface-wave recordings of NTS explosions. The authors concluded that the crust was about 30 km thick and relatively uniform with $\alpha = 6.1$ km/sec and $\beta = 3.6$ km/sec, except for a 1-km sedimentary layer at the surface. The P_n velocity was 7.9 km/sec, a typical value for the Basin and Range Province. Warren (1969) used refraction data to derive a model for central Arizona that is in basic agreement with that of Langston and Helmberger. He found the crustal thickness to increase from 21 km in southwest Arizona to 40 km in northeast Arizona, with the thickness being about 30 km where the profile crosses the NTS-TUC path. His model differs from that of Langston and Helmberger in having a high-velocity ($\alpha = 7$ km/sec) layer at the base of the crust.

Data from the NTS-ALQ path are less abundant, although there is agreement that the crust thickens from west to east. From refraction data, Prodehl (1970) found crustal thicknesses of 30 km near NTS and over 40 km in north-central Arizona. He found P_n velocities between 7.6 and 7.9 km/sec in northern Arizona. From a north-south refraction profile in central New Mexico, Toppozada and Sanford (1976) deduced a 40-km crustal thickness and a P_n velocity of 7.9 km/sec. Keller *et al.* (1976) inverted Rayleigh-wave group-velocity data from the Colorado Plateau, northeast of NTS. They found β increasing from 3.5 to 3.9 km/sec in a 40-km crust. From Love-wave phase velocities, Wickens and Pec (1968) estimated the average crustal thickness and uppermost mantle shear velocity between Dugway, Utah and Tucson to be 35 km and 4.4 km/sec, respectively.

Taking account of these other data, our models for the inversion of the phase and group velocities were constrained to have a low velocity sedimentary layer at the surface and a crust-mantle boundary at a specified depth. Poisson's ratio (ν) was fixed in the crust as were the α and ρ in the mantle. These constraints are summarized in Table 2.

How strongly do our models depend on the constraints in Table 2? First, the dispersion data are primarily controlled by β, so that α–β and ρ–β relationships do not greatly affect the ability of the inversion to find a model that fits the data. They serve mainly to guarantee a self-consistent model. Since our shortest period data

are at 5 sec, the data are also fairly insensitive to the sedimentary layer. The most important constraint is the crustal thickness. Trial inversions with crustal thicknesses much different from those in Table 2 gave models that were unable to fit the dispersion data as well and/or gave unacceptable values for the mantle velocity. Certainly the dispersion data could be fit with a smooth crust-mantle transition, but this would deny the existence of a P_n refractor.

The models inverted from the data are shown in Figures 3 and 4, together with a comparison of model phase and group velocities to the observations. An attractive

TABLE 2

CONSTRAINTS IMPOSED ON THE INVERSION

	ALQ	TUC
Sediment thickness	2.5 km	1.0
Crustal thickness	42.0 km	31.0
Crust	$\alpha = 1.695\beta$ ($\nu = 0.23$)	
	$\rho = 0.273\beta + 1.815$	
Mantle	$\alpha = 7.9$ km/sec	
	$\rho = 3.2$ gm/cm^3	

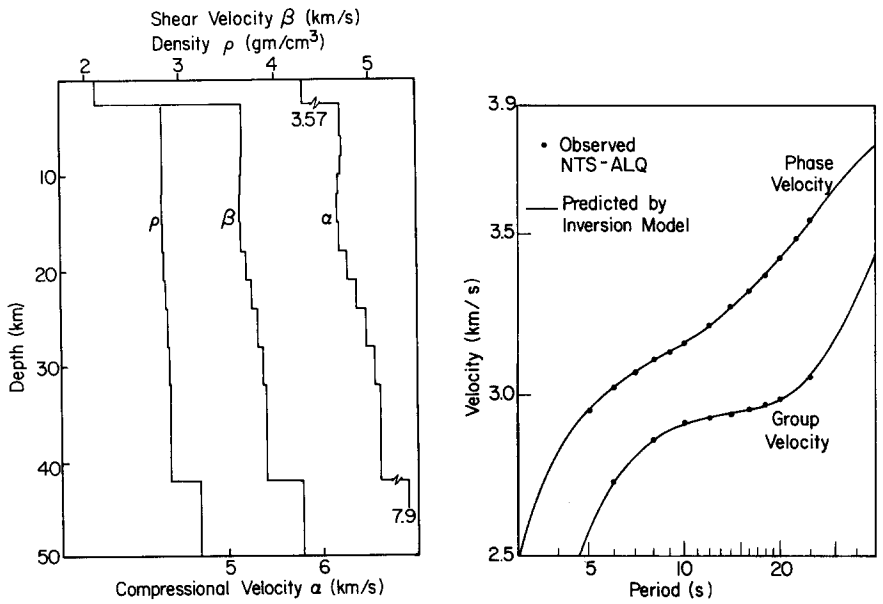

FIG. 3. The inversion model (*left*) for the NTS-ALQ path is shown together with a comparison of its predicted dispersion with the observed NTS-ALQ dispersion.

feature of these models is their simplicity; in fact, four-layer models would fit the data very well. Clearly, the models are in excellent agreement with the observed dispersion data; the largest residual is 0.01 km/sec. Further, both models are compatible with refraction data where it is available. However, we should point out that the refraction studies primarily determine the P velocity while our study primarily determines shear velocity.

The best-resolved portion of each model is that between 5 and 20 km. In this region our estimate for β at each depth is actually an average value over an 8-km interval and is determined to approximately 1 per cent (assuming the data are

accurate to 1 per cent). This resolving power is not enough to make the slight velocity minimum at 12 km in the NTS-ALQ model a significant feature. Also, the upper few kilometers of each model are poorly resolved, so the thickness and properties of this layer are not well-determined.

While it is difficult to resolve, a Conrad discontinuity in both models is suggested by the velocity increase in the lower crust. However, the gradual increase found by the inversion is an equally plausible feature.

A difficulty with interpreting the NTS-ALQ model is the evidence (from refraction studies) for a strong east-west variation in crustal thickness. The crustal thickness of our plane-layered model represents in some way an average of this lateral variation. A number of trial inversions were done with different crustal thicknesses and a tradeoff between crustal thickness and upper mantle shear velocity was found. A thin crust, say 35 km, results in an unreasonably low mantle shear velocity. On

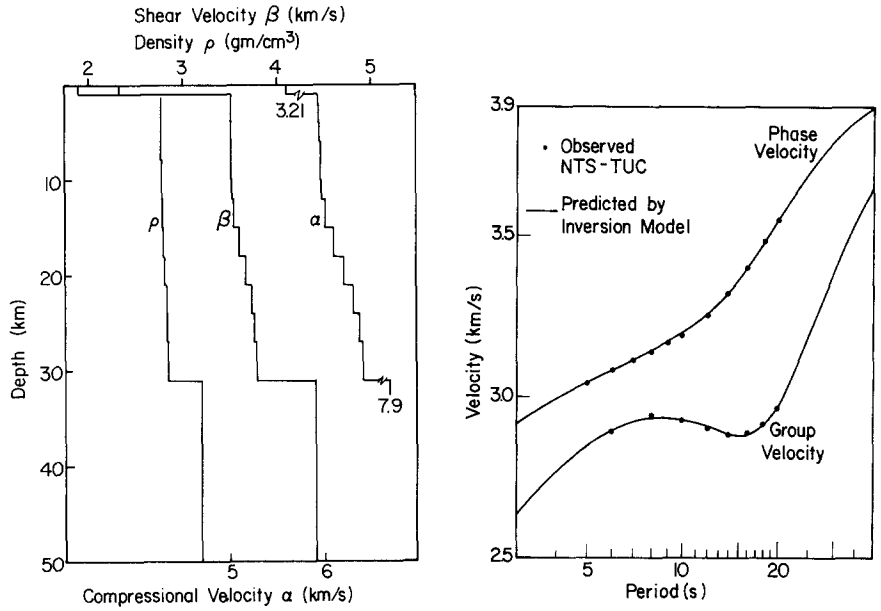

FIG. 4. The inversion model (*left*) for the NTS-TUC path is shown together with a comparison of its predicted dispersion with the observed NTS-TUC dispersion.

the other hand, a crustal thickness of 45 km or more gives a more reasonable mantle shear velocity, but seems too thick to be the average thickness for this path. The value chosen, 42 km, was judged best, though thicknesses a few kilometers different can also be justified.

Since the inversion determines the mantle shear velocity while the refraction data was used to fix the mantle P velocity, the mantle Poisson's ratio is a result of the inversion. Our mantle shear velocities are somewhat lower than those in other models (e.g., Langston and Helmberger, 1974), but still imply reasonable Poisson's ratios. For the NTS-TUC path $\beta = 4.4$ km/sec, $\nu = 0.27$ in the topmost mantle. The corresponding values for the NTS-ALQ mantle are 4.3 km/sec and 0.29.

CALCULATION OF THEORETICAL SEISMOGRAMS

Using equation (6) and the earth models of the previous section, we now calculate theoretical seismograms for comparison to the observations. The model for the

NTS-TUC path is thought to be the more appropriate for NTS, primarily because of its relatively thin crust. Therefore, for the source region we use this model, altering the top few kilometers to represent the specific test area (Climax Stock, Pahute Mesa, or Yucca Flat). The velocity-density profiles for this portion of the source models are shown in Figure 5.

From equation (6), when the path is fixed, the Rayleigh waves from explosions in different source materials are proportional to

$$\mu_s \hat{\Psi}(\omega) \frac{K_{s_1} \mathbf{A}_{R_1}}{c_1} T(\omega). \tag{11}$$

For the periods (>4 sec) and yields (50 to 500 kt) of interest, $\hat{\Psi}(\omega)$ is essentially equal to a constant, $\Psi(\infty)$, which represents the source coupling into elastic waves

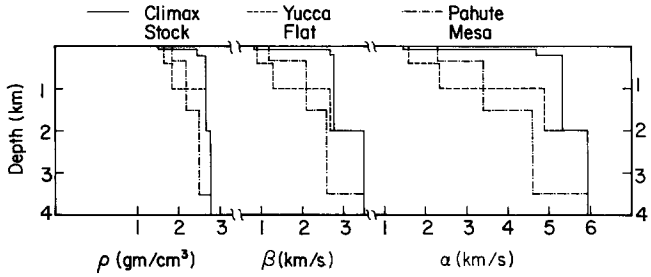

FIG. 5. The density, shear and compressional wave velocities are plotted versus depth for the three test areas at NTS. Below 3.5 km the source region models are the same as the NTS-TUC model in Figure 4.

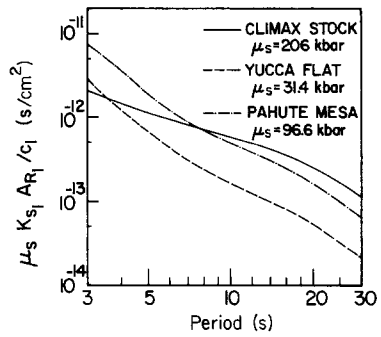

FIG. 6. The source amplification factor is shown for the three source areas studied.

and depends on the local rock properties (see Haskell, 1967; Bache *et al.*, 1975). Aside from this coupling term, the source excitation is given by $\mu_s K_{s_1} \mathbf{A}_{R_1}/c_1$ and is plotted in Figure 6 for the three test areas. The other quantity in equation (11), $T(\omega)$, is plotted in Figure 7 for the six source-path structure combinations. The $T(\omega)$ is intended to represent, albeit approximately, the transmission of Rayleigh waves from the source model to the path model. In Figure 7 we see that $T(\omega) = 1.0 \pm 0.15$ for periods greater than 5 sec for most of the paths. The exceptions, which are not severe, are for the ALQ path where the source and path models are quite different. Where $T(\omega)$ deviates substantially from unity, it is at least qualitatively correct, amplifying the waves generated in the high-velocity material and vice versa.

The relative source excitation terms (Figure 6) for Pahute Mesa and Yucca Flat

differ by a nearly constant factor over most of the frequency range. This constant is essentially the ratio of the shear moduli, the μ_s, for the two regions. On the other hand, the excitation function for the granite structure has a different period dependence and, for the range plotted, is much smaller than expected from the ratio of the shear moduli.

To complete the computation of theoretical seismograms, it is necessary to specify a Q or γ model. The models used are based on the western U.S. attenuation data of Mitchell (1975). Since these data were derived from observations of events in the Colorado Plateau, they were assumed to be appropriate for the NTS-ALQ path. Assuming Q is a function of depth and independent of period, these data were

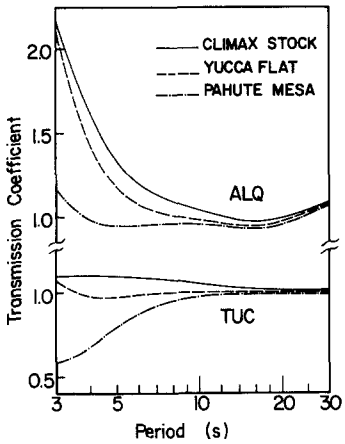

FIG. 7. The transmission coefficient $T(\omega)$ is plotted for the six source-path combinations studied.

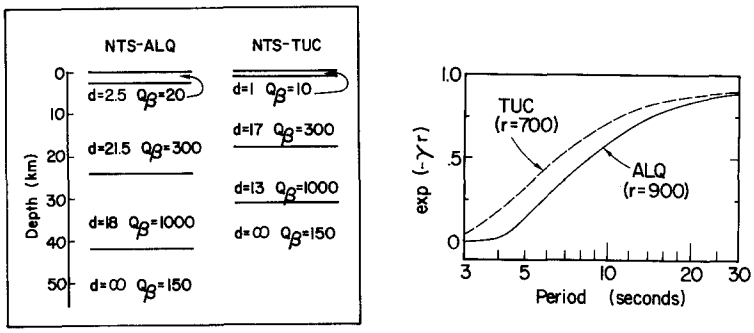

FIG. 8. The Q_β models used to derive $\gamma(\omega)$ are shown at left for the NTS-ALQ and NTS-TUC paths with d denoting layer thickness. At the *right* the amplitude attenuation is plotted for the two paths.

inverted for a four-layer NTS-ALQ Q model with layers corresponding to the distinct layers of our NTS-ALQ (α, β, ρ) model. We then assumed that the Q-β relationship was the same for the two paths and constructed a Q model for the NTS-TUC path. The Q models, which are different for the two paths (Figure 8), were used to compute $\gamma(\omega)$. Figure 8 also shows the resulting attenuation for the NTS-ALQ path (using 900 km as a representative distance) and for the NTS-TUC path (using 700 km).

COMPARISON OF THEORETICAL AND OBSERVED SEISMOGRAMS

Theoretical seismograms for the three events are compared to the ALQ and TUC observations in Figure 9. The wave-form agreement is remarkably good for all six

seismograms, even in some rather subtle details. One difference is in the half-cycle just ahead of the main pulse in the TUC seismograms which is too small in the synthetics. This may be due to the γ model or failure to precisely duplicate the Airy phase near 8 sec in the TUC dispersion. Aside from this, deviation between the two is either at periods (<5 sec) for which we could not extract dispersion data or, for ALQ, ahead of the main pulse where there is coherent energy that may be a higher mode Rayleigh wave. This comparison is an excellent check on the consistency of our approach.

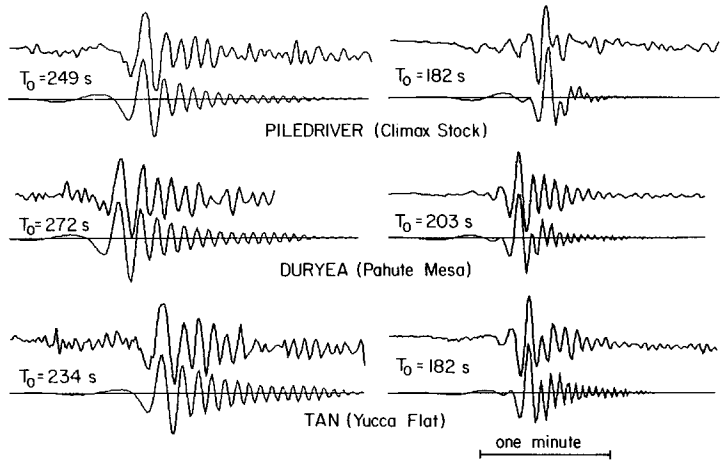

FIG. 9. Theoretical and observed seismograms are compared at ALQ (*left*) and TUC for events in three test areas at NTS. A bar indicating 1 min is shown. In each pair the observed (*top*) and theoretical records start at the same time with respect to the explosion detonation and this time is indicated as T_0.

CONCLUDING REMARKS

We briefly summarize the main features of crustal structure determination. A large number of recordings of NTS explosions at two WWSSN stations (ALQ and TUC) were collected and the wave forms were found to be quite consistent. For one event in three different test areas the records were digitized and analyzed to determine the phase and group velocities. For the phase velocities we used a straightforward unwrapping of the phase spectrum of the entire seismogram plotted in Figure 1 and no special windowing was found to be necessary. The group velocities were determined by a more sophisticated approach relying on the Hilbert transform envelope of the narrow-band filtered seismogram. The two sets of data were entirely consistent and varied little from event to event.

Using an average phase- and group-velocity curve from the data at each station, a linear inversion was done to determine the earth structure for the two paths. The models found agreed with the dispersion data with a maximum error of 0.01 km/sec. Further, these models are consistent with other available information on these paths, including that from refraction studies.

As an additional test of the models, synthetic seismograms were compared to the observations and the two were found to be in remarkable agreement. Thus, our models quite accurately account for the propagation of surface waves along these paths. Within the resolving power of the data and the restrictions imposed by the assumption of plane layers, the crustal structures in the regions sampled by the two paths must then closely resemble our models.

ACKNOWLEDGMENTS

It is a pleasure to acknowledge the assistance of our colleagues at Systems, Science and Software, especially Dr. John Savino, Dr. Joseph Masso, and Mr. David Lambert who did much of the data analysis. Dr. Charles Archambeau designed the MARS program used to determine group velocities. The inversion program used was developed in part while one of the authors (W. L. Rodi) was a student in the Department of Geosciences at The Pennsylvania State University. The authors are grateful to Dr. Brian Mitchell for providing a tabulation of his Western U.S. attenuation data. This research was supported by the Advanced Research Projects Agency of the Department of Defense and was monitored by the VELA Seismological Center under Contract F08606-76-C-0041 with Systems, Science and Software.

REFERENCES

Alewine, R. W. (1974). Application of linear inversion theory toward the estimation of seismic source parameters, *Ph.D. Thesis,* California Institute of Technology.

Alexander, S. S. (1963). Surface wave propagation in the western United States, *Ph.D. Thesis,* California Institute of Technology.

Bache, T. C., J. T. Cherry, N. Rimer, J. M. Savino, T. R. Blake, T. G. Barker, and D. G. Lambert (1975). An explanation of the relative amplitude generated by explosions in different test areas at the Nevada Test Site, *Systems, Science and Software Final Contract Report, DNA 3958F.*

Bache, T. C., J. T. Cherry, D. G. Lambert, J. F. Masso, and J. M. Savino (1976). A deterministic methodology for discriminating between earthquakes and underground nuclear explosions, *Systems, Science and Software Final Technical Report* submitted to ARPA, SSS-R-76-2925, July.

Backus, G. and F. Gilbert (1970). Uniqueness in the inversion of inaccurate gross earth data, *Phil. Trans. Roy. Soc. London, Ser. A.,* **266,** 123–192.

Diment, W. H., S. W. Stewart, and J. C. Roller (1961). Crustal structure from the Nevada Test Site to Kingman, Arizona, from seismic and gravity observations, *J. Geophys. Res.* **66,** 201–214.

Harkrider, D. G. (1964). Surface waves in multilayered media I. Rayleigh and Love waves from buried sources in a multilayered elastic half-space, *Bull. Seism. Soc. Am.* **54,** 627–679.

Harkrider, D. G. (1970). Surface waves in multilayered media II. Higher mode spectra and spectral ratios from point sources in plane-layered earth models, *Bull. Seism. Soc. Am.* **60,** 1937–1987.

Harkrider, D. G. and C. B. Archambeau (1978). Theoretical Rayleigh and Love waves from an explosion in prestressed source regions, (submitted for publication).

Haskell, N. A. (1967). Analytic approximation for the elastic radiation from a contained underground explosion, *J. Geophys. Res.* **72,** 2583–2587.

Johnson, L. E. and F. Gilbert (1972). Inversion and inference for teleseismic ray data, in *Methods in Computational Physics,* vol. 12, B. A. Bolt, Editor, Academic Press, New York, 231–266.

Jordan, T. H. (1973). Estimation of the radial variation of seismic velocities and density in the Earth, *Ph.D. Thesis,* California Institute of Technology.

Keller, G. R., R. B. Smith, L. W. Braile, R. Heaney, and D. H. Shurbert (1976). Upper crustal structure of the Eastern Basin and Range, Northern Colorado Plateau and Middle Rocky Mountains from Rayleigh-wave dispersion, *Bull. Seism. Soc. Am.* **66,** 869–876.

Langston, C. A. and D. V. Helmberger (1974). Interpretation of body and Rayleigh waves from NTS to Tucson, *Bull. Seism. Soc. Am.* **64,** 1919–1929.

McGarr, A. and L. E. Alsop (1967). Transmission and reflection of Rayleigh waves at vertical boundaries, *J. Geophys. Res.* **72,** 2169–2180.

McGarr, A. (1969). Amplitude variations of Rayleigh waves—propagation across a continental margin, *Bull. Seism. Soc. Am.* **59,** 1281–1305.

Mitchell, B. J. (1975). Regional Rayleigh wave attenuation in North America, *J. Geophys. Res.* **80,** 4904–4916.

Prodehl, C. (1970). Seismic refraction study of crustal structure in the western United States, *Bull. Geol. Soc. Am.* **81,** 2629–2646.

Rodi, W. L., P. Glover, T. M. C. Li, and S. S. Alexander (1975). A fast, accurate method for computing group-velocity partial derivatives for Rayleigh and Love modes, *Bull. Seism. Soc. Am.* **65,** 1105–1114.

Springer, D. L. and R. L. Kinnaman (1971). Seismic source summary for U.S. underground nuclear explosions, *Bull. Seism. Soc. Am.* **61,** 1073–1098.

Takeuchi, H., J. Dorman, and M. Saito (1964). Partial derivatives of surface wave phase velocity with respect to physical parameter changes within the earth, *J. Geophys. Res.* **69,** 3429–3441.

Toppozada, T. R. and A. R. Sanford (1976). Crustal structure in Central New Mexico interpreted from the Gasbuggy explosion, *Bull. Seism. Soc. Am.* **66,** 877–886.

Warren, D. H. (1969). A seismic-refraction survey of crustal structure in Central Arizona, *Bull. Geol. Soc. Am.* **80,** 257–282.

Wickens, A. J. and K. Pec (1968). A crust-mantle profile from Mould Bay, Canada, to Tucson, Arizona, *Bull. Seism. Soc. Am.* **58,** 1821–1831.

Wiggins, R. A. (1972). The general linear inverse problem: Implication of surface waves and free oscillations for earth structure, *Rev. Geophys.* **10,** 251–285.

SYSTEMS SCIENCE & SOFTWARE
P.O. BOX 1620
LA JOLLA, CALIFORNIA 92038 (T.C.B. & W.L.R.)

CALIFORNIA INSTITUTE OF TECHNOLOGY
SEISMOLOGICAL LABORATORY
PASADENA, CALIFORNIA 91125 (D.G.H.)

Manuscript received April 7, 1978